Optical Methods and Results of Dew Point and Deposition Rate Measurements in Salt/Ash-Containing Combustion Gases—$B_2O_3(l)$ Deposition Rates by Interference Methods and Comparisons with Theory

K. SESHADRI and D. E. ROSNER

Department of Chemical Engineering
High Temperature Chemical Reaction Engineering Laboratory
Yale University,
New Haven, CT 06520

This study is focused on deposition rate processes leading to inefficiency and "hot corrosion" in fossil-fuel-fired furnaces and engines. The inorganic compounds which deposit on heat exchanger surfaces and blades are formed in combustion product gases when the fuel and/or ingested air contains inorganic impurities. An improved understanding of the coupled thermodynamic, kinetic, and transport processes governing the deposition rate of inorganic oxides and salts from hot gases containing these compounds (or their precursors) can suggest more efficient test strategies and control measures. Accordingly, an optical interference method for accurately measuring the growth rate of deposits well before the onset of run-off under laboratory burner conditions has been developed.

To demonstrate the technique and provide data suitable for theoretical model development, a deliberately simple chemical system and target geometry are used. $BCl_3(g)$ is introduced into a premixed C_3H_8-air flat flame at atmospheric pressure. The growth rate of $B_2O_3(l)$ on an electrically heated platinum ribbon is then measured interferometrically over a range of fuel/air ratios and seed levels. However, the very existence of $B_2O_3(l)$ deposition at the present seed levels and surface temperatures (about 1,200–1,300 K) clearly demonstrates the importance of kinetic restrictions on $B_2O_3(l)$ gasification reactions. Optically measured film growth rates are obtained at film thicknesses small enough to neglect condensate run-off, hence they yield vapor deposition rates directly. These deposition rates are found to be in good agreement with the predictions of a recently developed multicomponent mass-transfer boundary layer (*BL*) theory, with a constrained equilibrium ($(HBO_2)_3$ precluded) boundary condition. Remarkably, at a constant value of the BCl_3 flow rate, the Pt ribbon temperature above which there is no B_2O_3 condensate (i.e., the so-called dew point) is observed to depend on the fuel/air ratio. Whereas previous equilibrium-based deposition models cannot embrace such phenomena, a semiquantitative argument, based on the nonequilibrium chemistry of B_2O_3 precursor formation and $(HBO_2)_3$-formation barriers, explains these potentially significant trends. These encouraging results suggest a more general applicability for the optical methods and chemically frozen (*CF*) *BL* theory described herein, and demonstrate the important role of heterogeneous and homogeneous kinetic barriers in determining dew points and deposition rates in combustion systems.

SCOPE

With increased interest in the combustion of minimally processed coal-derived fuels and lower grade residual fuel oils, the problems attending inorganic salt and ash deposition on heat exchanger surfaces, turbine blades, etc. assume greater importance. However, an understanding of the laws governing deposition has been impeded by the lack of precise and rapid methods of deposition rate measurement—with some experiments lasting more than 12 hours each and yet being clouded by the effects of liquid condensate run-off. To provide improved methods and the data to test recently developed multicomponent convective-diffusion mass transfer theories, we have invoked real-time optical laser reflectance-interference techniques in high-temperature combustion environments.

CONCLUSIONS AND SIGNIFICANCE

Based on the present B_2O_3 deposition experiments using a $BCl_3(g)$-seeded laboratory flat flame burner, we have concluded that: (a) laser-optical techniques can be extended to combustion systems by remotely probing ribbon targets for the onset of condensation (dew point) and determining condensation rates interferometrically, here on a 10 second time scale and well before the onset of surface flow phenomena; (b) the dew point is not dictated only by thermodynamic factors, but is strongly influenced by transport and kinetic restrictions, the latter evi-

K. Seshadri is presently at the University of California, San Diego, CA.
Correspondence concerning this paper should be directed to D. E. Rosner.

dently existing both in the vapor phase, and at the vapor/condensate interface; (c) and optically inferred deposition rates for $B_2O_3(l)$ are in approximate accord with a multicomponent mass transfer theory recently developed by D. E. Rosner. Even for a single-component condensate (as in the present experiments) it is shown that a multicomponent vapor transport formulation is essential since the species responsible for transport are generally stoichiometrically different from the growing condensate; i.e., heterogeneous and/or homogeneous chemical reactions are involved in such vapor deposition. These new techniques and data provide the basis for an improved understanding of deposition rate phenomena in engines, boilers, and simulation test facilities, as well as the basis for a family of new on-line control instruments.

INTRODUCTION

Fossil fuels as well as the air ingested for combustion contain inorganic impurities which inevitably lead to the formation of inorganic salts and/or "ash" in furnaces and engines. Once condensed, these compounds often foul and/or corrode surfaces exposed to such combustion product gases. For example, an accelerated sulfidation, called "hot corrosion," is associated with $Na_2SO_4(l)$ on gas turbine (GT) blades (Stringer, 1977) when the fuel contains sulfur (about 0.02–1.0% by element wt.) and the intake air contains sodium chloride (about 0.01–10 ppm by wt., as in the marine environment). Similarly, aggressive condensates result from the presence of vanadium in fuel oil, and ash and sulfur in coals used for conventional power generators (Boll and Patel, 1961; Jackson, 1977) or magneto-gas-dynamic (Dicks et al., 1977; Heywood and Womack, 1969) types. [See Halstead and Raask (1969), Stearns et al. (1982), and Hedley et al. (1966) for a useful overview of this area.] Current trends in the supply and synthesis of fuels indicate that these problems will intensify in the next two decades. Moreover, effectively implementing any one of such control strategies as a) fuel pretreatment, b) fuel additives, c) altered deposition conditions, and/or d) the development of more corrosion-resistant high-temperature alloys, will require an improved understanding of the kinetics, thermochemistry and dynamics of salt/ash formation and deposition. As in earlier papers in this series (Kohl et al., 1979; Rosner et al., 1979a,b; Rosner and Seshadri, 1981), the present paper is focused on the physical and chemical *deposition* processes leading to liquid condensate layers on metal surfaces exposed to high-temperature combustion products—such layers indeed appear to be necessary to the observation of corrosive attack in GT and similar applications (DeCrescente and Bornstein, 1969). These convective mass transfer studies are also of fundamental interest, providing further insights into the coupling between gas dynamic, transport and chemical kinetic phenomena.

Chemically Frozen Multicomponent Mass Transport Theory

A general theory for predicting condensate growth rates on surfaces exposed to combustion product gases containing these substances and/or their precursors in vapor or submicron aerosol form has been developed by Rosner et al. (1979a) and is summarized below. Accurate measurements of condensate layer growth rates under well-controlled laboratory conditions are essential to test the applicability of this theory so that: a) it can be extended with confidence to predict growth rates in situations less accessible to direct experimental methods, and b) used to evaluate future control strategies.

Definitions

The surface on which condensation and growth occurs will be called the *target*, and the target temperature, T_{dp}, above which no condensate appears for a given set of experimental conditions will be called the dew point (dp). By *seed material* we imply one (or more) compound(s) added to the fuel and/or oxidizer to serve as a precursor to the inorganic salt ultimately formed on the target. Of principal interest will be the *deposition mass flux from the vapor*, i.e., a quantity which can be measured by following the rate at which the deposit thickens at target temperatures between T_{mp} and T_{dp}, provided surface flow effects (condensate run-off due to aerodynamic shear and/or surface tension gradients) are negligible. [See Appendix B and Rosner, Günes and Anous (1983).]

Previous Experimental Data

Previous measurements of dew points and deposition rates of inorganic salts on surfaces immersed in combustion product gases were made using gravimetric techniques (Hedley et al., 1966; Brown, 1966; Laxton et al., 1978; Kohl et al., 1979), i.e., weighing the deposits collected after many several hours of exposure. The present experimental work was undertaken to: a) expand the parameter range covered (fuel type, mixture ratio, seed level/type); b) avoid the complexities of data interpretation associated with condensate run-off above the melting point; and c) improve the data precision [to provide more meaningful comparisons with predictions based on the recently developed chemically frozen boundary layer ($CFBL$) theory (Rosner et al., 1979a)] and acquisition rate.

Optical Methods

To accurately and conveniently measure dew points and deposition rates in a high-temperature combustion environment, we have chosen and adapted optical probing methods (Rosner et al., 1979b; Rosner and Atkins, 1983). For transparent condensates on highly reflecting targets, such measurements can be made by two methods, referred to hereafter as the *interference* method and the *ellipsometric* method (Seshadri and Rosner, 1984). The simpler interference method was used to obtain the results given herein. [McIntyre and McTaggart (1970) used interference in unpolarized reflected sodium vapor lamp radiation to study solid iodide film growth on silver in a low-pressure flow reactor. Sugawara et al. (1973) exploited the optical interference principle to study SiO_2 growth rates on silicon wafers using He-Ne laser radiation.] These methods follow in "real time" the deposit growth rate when the condensate layer is only of the order of 1 μm thick—usually well before the onset of complicating condensate *flow* (e.g., run-off) phenomena when the surface is above the deposit melting point [See Appendix B, and Rosner, Günes and Anous (1983).]

Choice of System

Measurements of deposition rates using seed compounds introduced as *liquid* solutions inevitably include some uncertainty in the seed concentration entering the flame reaction zone (a non-negligible fraction of the liquid solution introduced may adhere to the burner walls and escape entry). To avoid this difficulty and even more serious problems in introducing *solid* powders, we introduced a *gaseous* compound, boron trichloride (BCl_3), into a propane-air premixed flame. Oxidation of the added BCl_3 resulted in the formation of boric oxide precursors in the flame. Hot corrosion in current engineering applications is, of course, not due to condensed boron compounds—we used BCl_3 (g)-seeding to demonstrate the feasibility and power of the optical method to determine deposition rates under combustion conditions. Our focus on the *deposition* process allowed us to also eliminate the complication of the simultaneous metal corrosion via the use of platinum as the target material. We believe these results can be extended to other chemical situations, once the validity of the underlying mass transport theory is established (Rosner and Atkins, 1983).

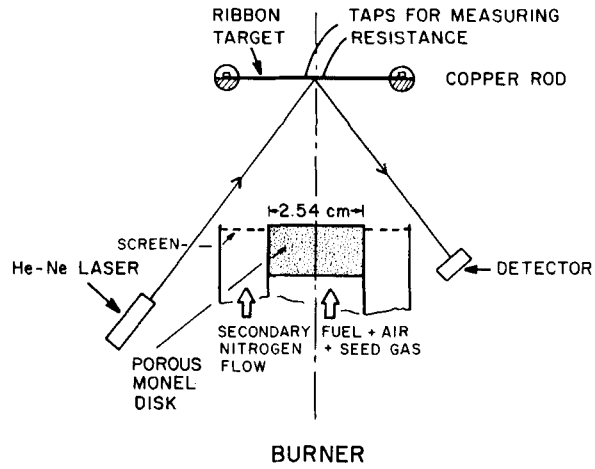

Figure 1. Experimental arrangement showing the inorganic vapor-seeded flat flame burner and optical system for dew point and deposition rate measurements (schematic).

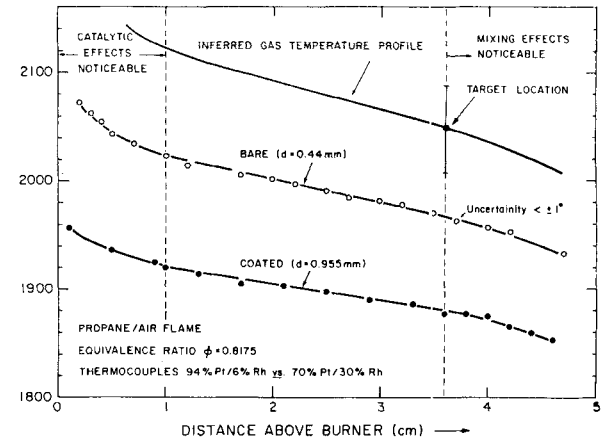

Figure 2. Measured gas temperature profiles above the burner (via coated and bare Pt 6% Rh vs. Pt 30% Rh thermocouples).

MEASUREMENTS OF DEW POINTS AND DEPOSITION IN COMBUSTION ENVIRONMENTS BY OPTICAL METHODS

The simplest configuration consistent with the use of the optical interference method proved to be that of an electrically heated platinum ribbon target immersed transverse to the combustion products of a seeded flat flame burner (Figure 1).

Apparatus

The apparatus consists of: a) an optical system, b) an electrical system for target heating and temperature measurement, c) the burner assembly, and d) the gas feed system.

Optical System. The optical arrangement (Figure 1) incorporates a linearly polarized helium-neon laser with an output power of 2 mW to supply an intense, collimated beam of monochromatic light (0.6328 μm) incident upon the center of the deposition target. The intensity of the specularly reflected beam was then measured and recorded via a photometer-potentiometer combination.

Electrical System. The target was a taut platinum ribbon (5 cm long,) 6 mm wide and 0.127 mm thick). The ribbon was held above the burner by two copper rods (Figure 1), connected to a DC power supply, which can deliver up to 50 A and 50 V at constant current or constant voltage. The ribbon temperature can be continuously changed by varying the electrical power supplied. Two platinum wires of 0.127 mm diameter, spot-welded across a 4 mm central section of the ribbon, were used to measure its electrical resistance, and hence temperature of this section. For this purpose a calibration curve relating the ribbon electrical resistance to its temperature was obtained by also measuring its brightness temperature with an optical pyrometer. Our measurements agreed with those reported earlier by Nordine et al. (1973). The target brightness temperature showed negligible variation ($\leq$5 K) between the voltage taps and across its width. (See Appendix B.) Reported dew point and deposition rate measurements pertain to this virtually isothermal portion of the ribbon.

Burner and Gas Feed. The flat flame burner was fabricated from a 2.54 cm (ID) stainless-steel tube. A premixed gaseous stream of fuel (C_3H_8), air and the seed gas (BCl_3) was fed to the burner at its base. Variable area flowmeters were used to measure gas flow rates, with uncertainties less than ±2% of full scale. To obtain a laminar flow of the premixed gases with a uniform velocity above the burner, porous stainless steel discs were placed on its top (Figure 1). To improve the stability of the flame and to delay the influx of atmospheric oxygen into the combustion products, a "curtain" flow of gaseous nitrogen was maintained.

Selection of Target Location

Two competing factors affect the optimum location of the target above the burner surface. First, since the Pt target material can itself catalyze chemical reactions, it should be placed sufficiently far downstream from the burner surface to allow the composition of the reacting gas mixture to attain chemical equilibrium at the local gas temperature. However, the flow field ultimately becomes unsteady and nonuniform as this distance increases. To find the best axial target location gas temperature measurements were made with a bare Pt 6% Rh vs. Pt 30% Rh thermocouple, and with a similar thermocouple, coated with a layer of Y_2O_3 (Kent, 1970) to suppress catalytic effects. Reproducibility of the resulting measurements (Figure 2) was better than ±1 K. We note that coated thermocouple temperatures are lower than those for the bare thermocouple primarily because its bead diameter and emittance (d = 0.95 mm ϵ = 0.28) are larger (*cf.* 0.44 mm, 0.2), resulting in higher relative radiation losses. [A value of 0.28 at 1,900 K for the total normal emittance of yttrium oxide was estimated by extrapolating data given—between 900 and 1,300 K, from Touloukian and DeWitt (1972). The total normal emittance of 0.2 for platinum at 1,900 K was obtained from Touloukian and DeWitt (1970).] The temperature profiles show identical slopes at all locations except between 0 and 1 cm above the burner surface, suggesting some localized catalytic recombination heating effects there. The two profiles also show a noticeable change in slope beyond about 3.8 cm presumably the location of appreciable secondary nitrogen entrainment. For these reasons the target was placed 3.8 cm above the burner. In addition, these profiles show that small errors in axial location of the target will produce insignificant uncertainties in the prevailing mainstream gas temperature, T_∞, calculated by equating the convective heat transfer to the radiative heat loss for each of the two-size thermocouples. Horizontal (radial) temperature profiles at 3.8 cm were found to vary less than ±5 K over a radius of 6 mm from the burner axis. Therefore, at this target location the gas temperature varies negligibly over the area where the following dew point and deposition rate measurements were made.

Procedure for Dew Point and Deposition Rate Measurement by Reflected Light Interference Technique

The monochromatic laser light is focused on the Pt ribbon between the voltage taps and the intensity of the specularly reflected light is monitored on the recorder via the photocell detector. The air and propane rates are adjusted to predetermined values, and the flame ignited. Initially the ribbon is maintained several hundred degrees above the B_2O_3-dew point at the anticipated BCl_3-seed level. The seed gas is then turned on, forming boric oxide precursors in the flame. When the ribbon heating current is abruptly reduced, bringing it below the prevailing B_2O_3-dew point, a sharp decrease in the reflected light intensity is observed at the instant of oxide condensation. Moreover, as the oxide film grows, the light reflected from its outer and inner (ribbon) surface undergoes constructive and destructive interference, causing a

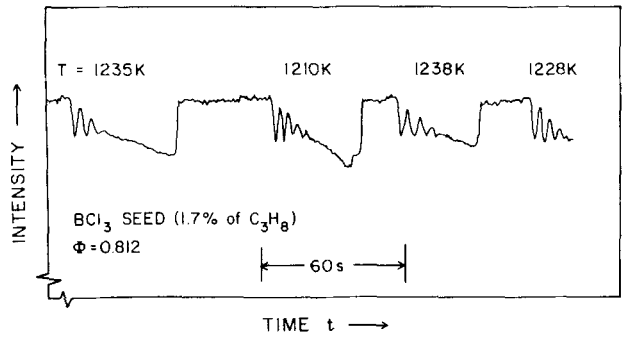

Figure 3. Interference patterns obtained on a growing B_2O_3 film (recording potentiometer output).

modulated intensity in the collected beam. The ribbon heating current is then increased to evaporate this oxide layer, and the experiment repeated to obtain the growth rate at a different target temperature. A typical output from the recording potentiometer is shown in Figure 3. The film thickness increment $\Delta\delta_l$ associated with a change from an intensity maximum to a minimum is calculated from:

$$\Delta\delta_l = 1/4\,(n^2 - \sin^2\theta)^{-1/2} \cdot \lambda \qquad (1)$$

where λ (0.6328 μm) is the laser light wavelength, n (=1.458) is the $B_2O_3(l)$ refractive index at this wavelength (Samsonov, 1973) and θ the angle of incidence. [The composition of the deposit was confirmed to be B_2O_3 by subsequent (X-ray photo-electron spectrometer (*XPS*)) analysis.] Results for B_2O_3 dew points and deposition rates measured at different flow rates by this technique are shown in Figures 4 to 6 and 8. Uncertainties in deposition rates, estimated to be ±5%, are attributed primarily to errors in manually measuring the distance between the light intensity maxima and minima from the chart recorder output (Figure 3). In Appendix B we demonstrate that, despite the liquid state of the B_2O_3 condensate, these growth rate measurements are not complicated by surface film *flow* phenomena, which, under the present circumstances, would set in only at film thicknesses well above 10 μm. Uncertainties in target temperature are estimated to be ±10 K and are attributed to systematic changes in specimen geometry (hence room temperature electrical resistance) during the experiment. Reproducibility of the target temperature measurements was better than ±2 K.

THEORY

General Formulation

The mass transport theory on which the analysis of these experiments is based has recently been described in detail (Rosner et al., 1979a). While straightforward, the formulation is general enough to predict salt/ash deposition rates under both combustor and laboratory test conditions. Provision is explicitly made for the following essential features:

Multicomponent Transport. At combustion gas temperatures the chemical elements which ultimately appear in the condensate are generally present in many compounds which act as condensate precursors. Accordingly, the theory incorporates the multicomponent nature of element transport in this class of problems.

Thermal (Soret) Diffusion Mass Transfer. The inorganic salt or oxide vapors, particles and their precursors are often characterized by molecular weights very different from that of the "host" combustion gas mixture. [Soret mass transport can also be quite important in the *surface-catalyzed combustion* of light weight (e.g., $H_2(g)$) or "heavy" weight molecular species (e.g., $C_{10}H_{22}(g)$) in air. Such "hot wall" cases have directly been examined in detail by R. Israel (1983) for both forced and natural convection.] Whenever there is also a significant BL temperature gradient this produces a nonnegligible thermal (Soret) diffusion contribution to the species flux (Rosner, 1980). While the theory is capable of including Soret or thermophoretic transport in a simple manner

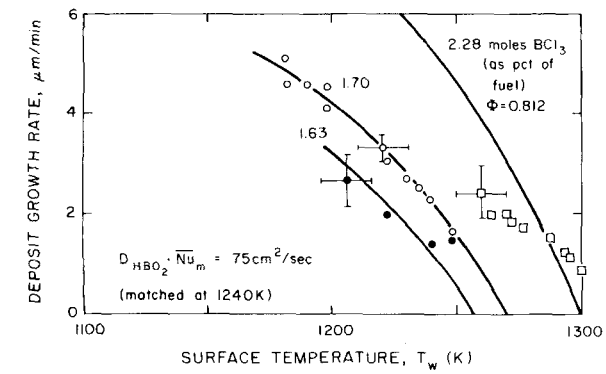

Figure 4. Experimental measurements (with target temperatures calculated *using 0.3 for the spectral emittance of platinum*) of $B_2O_3(l)$ liquid layer growth rates. Solid curves are theoretical predictions of $B_2O_3(l)$ *deposition* rates (Appendix B) for nonequilibrium concentrations of HBO_2 at the vapor/liquid interface.

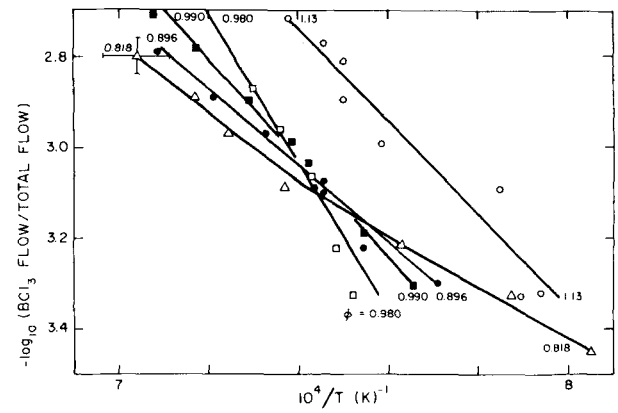

Figure 5. Experimentally measured dew point of B_2O_3 at different BCl_3-seed levels and flame equivalence ratios, φ.

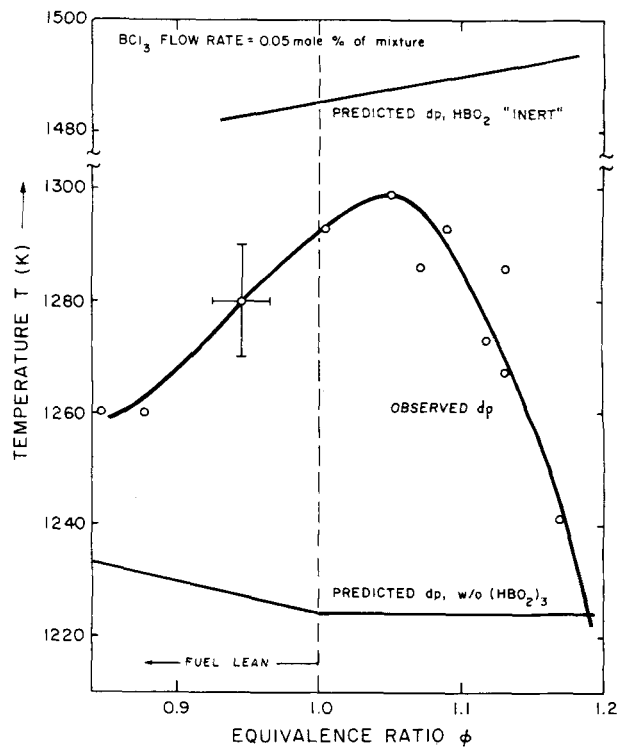

Figure 6. Experimentally measured and theoretically estimated B_2O_3-dew point at constant BCl_3 seed level.

(Gokoglu and Rosner, 1984), for the B_2O_3-deposition experiments described here this particular effect is negligible.

Variable Properties. Because the target temperature is lower than that of the combustion products, gas properties (transport and thermodynamic) vary across the BL. This affects the dimensionless *mass* transfer coefficients in a manner somewhat different from the (better-known) dimensionless *heat* transfer coefficients. Pending additional experimental data, this effect can be estimated based on exact solutions to the laminar BL equations under comparable conditions (Rosner et al., 1982).

Free Stream Turbulence. Although the flow in our experiments is laminar, in most practical situations the mainstream is turbulent. In such cases time-average transport rates can be estimated using empirically-determined Nu-enhancement factors.

To simplify our computations without sacrificing their realism, several assumptions were made. The resulting theoretical predictions are in reasonable agreement with our experimentally inferred B_2O_3-deposition rates. We assume that: 1) the mainstream temperature is high enough to preclude the existence of *condensed* inorganic compounds, and kinetic or thermodynamic barriers preclude their appearance within the vapor *BL;* 2) negligible (homogeneous) chemical reaction occurs within the *BL* adjacent to the target. Thus, we deal with the tractable limiting case of a single-phase "chemically frozen" boundary layer (*CFBL*) within which convection, concentration (Fick) diffusion and thermal (Soret) diffusion participate in species mass transport to/from the surface. Our deposition rate data suggest that these assumptions provide a reasonable starting point, especially for highly undersaturated mainstreams of a dilute condensible vapor, and surfaces which are not strongly (actively) cooled (Rosner and Epstein, 1968).

For each trace species, i, characterized by local mass fraction ω_i, the diffusion flux law for mass transport can be approximated by:

$$\vec{j}_i'' = -D_i\rho[\mathbf{grad}\ \omega_i + \alpha_i\omega_i\ \mathbf{grad}\ ln\ T] \tag{2}$$

where the Soret effect is included but body force and pressure diffusion are omitted. [As is well known, in deposition situations involving dispersed condensates in high-speed streams, particulate mass transfer *is* influenced by the inertial "slip" of the particle phase in the prevailing decelerating carrier fluid. Interestingly enough, the onset of this phenomenon is fully equivalent to *pressure diffusion* (Fernandez de la Mora and Rosner, 1982), but the "diffusion" description fails near the onset of actual "inertial impaction" on the target. Under our present experimental conditions (flow rates, target size), such "inertial" effects would be negligible even for micron-sized particles in the mainstream (Rosner and Atkins, 1983). They are, therefore, certainly negligible for the transport of "high" molecular weight vapor species (e.g., $HBO_2(g)$) here responsible for deposition.] Here we exploit the fact that in most practical situations, including even our experimental conditions, the inorganic compounds participating in the deposition process predominantly collide with the "host" (combustion product) gas. On this basis algebraic expressions for each $j_{i,w}''$ can be written which explicitly correct both the transfer coefficient and the driving force for the effects of Soret transport (Rosner et al., 1979a; Rosner, 1980). When these effects are negligible we recover the well-known separable form:

$$-j_{i,w}'' = [(D_i\rho)_e/L] \cdot [Nu_{m,i}\{x/L, Re, Sc_i, T_w/T_e\}] \cdot [\omega_{i,e} - \omega_{i,w}] \tag{3}$$

where the subscripts e and w, respectively, pertain to local conditions at the outer and inner edges of the gas *BL*.

Application of Theory to Boric Oxide Deposition

At the *BL* outer edge, i.e., at station e, the element boron, which ultimately appears in the deposit $B_2O_3(l)$, is distributed over the gaseous species HBO_2, BO_2, B_2O_3, HBO, BOCl, BO . . . If we make the simplest and often realistic assumption that local thermochemical equilibrium (*LTCE*) is achieved at station e, the corresponding species concentrations $\omega_{i,e}$ can be computed, e.g., by employing the free-energy minimization program of Gordon and McBride (1971). However, at the surface of the target, station w, we shall later that $\omega_{i,w}$ is probably not in *LTCE* for some chemical species. This not only implies that the surface is unable to bring about *LTCE*, but also that there is insufficient *BL* residence time for equilibration by homogeneous chemical reactions. Nevertheless, at station w, the following two conditions are imposed:

1. *Vapor-Liquid Equilibrium* (*VLE*). We assume that the vapor mixture composition at station w is compatible with the thermochemical coexistence of $B_2O_3(l)$ at temperature T_w.

2. *Flux-Ratio Constraints.* The element ratios at the station w will, in general, be different from those at station e; "element segregation" occurs across such boundary layers. The element ratios at the wall must, in fact, be such that the net flux of the element chlorine to the wall is zero, and the ratio of the mass flux of element boron and element oxygen must be the same as the mass ratio between these elements in the condensate $B_2O_3(l)$. One self-consistent procedure for incorporating such flux-ratio constraints is outlined by Rosner et al. (1979a). However, application of the theory to available Na_2SO_4-deposition experiments (Kohl et al., 1979; Rosner et al., 1979a), have shown that element segregation due to thermal and multicomponent diffusion only slightly altered deposition rates far below the dew point and altered the dew point itself by less than 10 K. Therefore, for simplicity, the element flux constraints were suppressed in these calculations.

Estimates of the thermodynamic and transport properties of the individual species, and for the gas mixture, were made by employing procedures similar to those described by Rosner et al. (1979a). Estimates of the diffusion coefficient D_i for some species proved to be more complicated in this system, Appendix A. Appendix A also describes our procedure to estimate the dimensionless mass transfer coefficients $Nu_{m,i}$ for the front surface of the ribbon.

Assembling this information, the total diffusional flux of the element boron to the surface can be obtained from a weighted sum of the fluxes of all boron-containing species,

$$j_{(B),w}'' = \sum_i \omega_{B/i} j_{i,w}'' \tag{4}$$

where $\omega_{B/i}$ is the fraction of the mass of molecule i contributed by the element boron. Again exploiting the diluteness assumption, the corresponding mass flux of $B_2O_3(l)$ at the wall can, therefore, be written:

$$-\dot{m}_w'' = -j_{(B),w}''/\omega_{B/B_2O_3(l)} = 6.440(-j_{(B),w}'') \tag{5}$$

Equations 3 to 5 were used to calculate the expected $B_2O_3(l)$ film growth rates before the onset of surface flows (Appendix B)—corresponding to those inferred using the optical interference technique.

EXPERIMENTAL RESULTS AND INTERPRETATION

Experimental Results

Results for the $B_2O_3(l)$ film growth rates measured at different initial concentrations of BCl_3-seed in the fuel-air mixture are shown in Figure 4. These measurements were made at constant *flame equivalence ratio* ϕ (ratio of the *prevailing* fuel/air ratio to the *stoichiometric* fuel/air ratio). The results show that at a constant BCl_3 seed flow rate the deposition rate increases with decreasing target temperature, and both the deposition rate (at constant target temperature) and dew point increase with increasing BCl_3 seed level. Figure 5 shows the corresponding results for the reciprocal of the experimentally measured B_2O_3-dew points as a function of the logarithm of the fractional BCl_3-flow rate (volume flow rate of BCl_3/total volume flow rate of mixture). The value of the dew point (dp) obtained by extrapolating the deposition rate curve shown in Figure 4 is actually somewhat lower than the dew point (dp_+) measured by slowly cooling the target and recording its temperature at the onset of boric oxide condensation, Figures 5 and 6. Although such differences are small (30–40 K), they are not unexpected (Rosner et al., 1979a; Rosner and Nagarajan, 1983). As would be expected for the deposition of a pure, "nonparticipating" vapor,

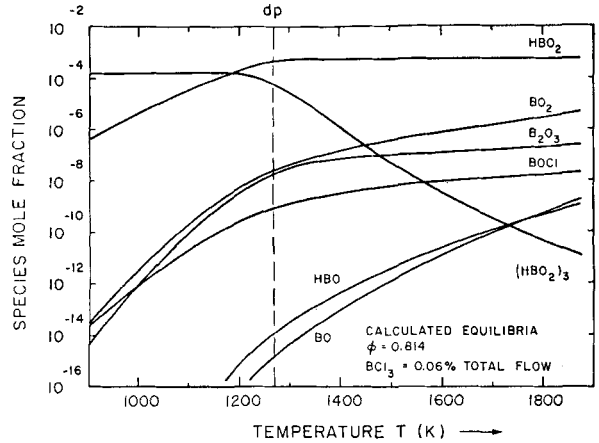

Figure 7. Calculated equilibrium concentrations of boron-containing species at $\phi = 0.814$ for a BCl_3 seed level of 0.06% of the total flow.

at constant ϕ the results fall on a straight line. However, *the slopes are surprisingly ϕ-dependent*, reflecting the complex seed and combustion gas chemistry. From this plot, it appears that if the logarithm of the fractional flow rate of boron trichloride is held at a constant value below −3.2, the measured dew point maximizes for a nearly stoichiometric fuel/air mixture. To check this expectation, we measured the B_2O_3 dew point directly as a function of ϕ, at constant fractional BCl_3 flow rate. The results in Figure 6 reveal that the dew point is indeed a maximum at $\phi \approx 1.05$. For values of $\phi \geq 1.2$ boric oxide did not condense on the ribbon, even at its lowest steady-state temperature (1,023 K with no electrical heating). Reproducibility of the measurements of T_{dp}, ϕ and fractional BCl_3 flow rate is better than 0.4%, 1%, and 1%, respectively.

Dew Point Predictions Based on Partial Equilibrium at Surface

Local thermochemical equilibrium (*LTCE*) calculations at the experimentally measured relative flow rates of air, propane, and boron trichloride were made to gain an understanding of the factors governing the experimentally measured B_2O_3 dew point. These calculations for atmospheric pressure and various temperatures employed the *LTCE* computer program of Gordon and McBride (1971). This program is capable of calculating the equilibrium composition of a reacting gas mixture for assigned thermodynamic conditions. Typical program input would be the initial (unreacted) mixture composition and the thermodynamic state of each reactant (via two thermodynamic state functions). The program minimizes the mixture free energy considering over 500 species from the JANAF tables (Stull, 1971). The *LTCE* results (Figure 7) clearly show that at the BCl_3-seed levels used in our experiments, equilibrium thermodynamics predicts that boric oxide condensate should *not* be present for values of temperature even as low as 300 K. Figure 7 also shows that if the system is in *LTCE* metaboric acid (HBO_2) is the major boron-containing vapor species at temperatures above the measured dew point, while the trimer of metaboric acid $(HBO_2)_3$ should dominate (B)-transport below it. Comparing these calculations with our observations suggests that significant departures from *LTCE* exist in our system, either in the mainstream (outside the *BL*) and/or at the target surface. Experimental measurements of the reaction velocities of $BCl_3(g)$ with oxygen (Geiss and Frosche, 1976) suggest that in our system there is enough residence time (9.2 ms) to achieve *LTCE* in the mainstream at the target position for these homogeneous chemical reactions, implying that *LTCE* departures exist near and at the target surface. Interestingly, previous experimental measurements of gaseous species in the presence of condensed boric oxide between 1,060 and 1,450 K (Meschi et al., 1960) revealed a lack of chemical equilibrium. Specifically, the $(HBO_2)_3$-concentration was measured to be much lower than its equilibrium value. In view of these measurements, we made species concentration calculations based on the assumptions of: 1) *LTCE* at the mainstream (about 2,120 K from Figure 3) and target (below 1,450 K); 2) $(HBO_2)_3$ is not formed. Resulting values of temperature above which boric oxide is entirely in the gaseous form (shown in Figure 6 vs ϕ) are within 75 K of the measured dew point. These observations reinforce our view that while an unambiguous *thermodynamic* dew point can usually be defined and calculated (Prausnitz et al., 1967), even in high-temperature engineering systems the observed dew point can be drastically affected by kinetic and transport limitations, in addition to the prevailing thermodynamics.

Theoretical Prediction of Deposition Rates

The *CFBL* theory discussed earlier has been used to predict B_2O_3-deposition rates under conditions corresponding to our experimental measurements. The surface temperature at which the deposition rate of B_2O_3 is zero, obtained by extrapolating the experimentally measured B_2O_3 film growth rates, Figure 4, was found to be about 15 K higher than the theoretical "partial" equilibrium thermodynamic $B_2O_3(l)$ dew point (with $(HBO_2)_3$ disallowed.

A difference of only 15 K in dew point can be easily attributed to experimental uncertainties ordinarily encountered in the measurement of high temperatures, even using Pt resistance thermometry. Thus, values quoted (Lyman, 1975; Washburn, 1929) for the temperature coefficient of electrical resistance of platinum are not applicable when the specimen is exposed to oxidizing atmospheres and the temperature is above 1,273 K (Fryburg and Petrus, 1961; Nordine et al., 1973). Specifically, in obtaining the calibration curve relating the electrical resistance of the platinum ribbon to its temperature, the latter quantity was measured with an optical pyrometer. Emittance corrections to the observed "brightness") temperature were initially calculated using a literature value of 0.3 for its spectral emittance at 0.65 μm (Lyman et al., 1975).

Since the spectral emittance of platinum can change with temperature and gaseous environment [the 0.65 μm emittance of platinum in inert atmospheres varies between 0.3 and 0.42 between 1,000 and 1,500 K (Touloukian and DeWitt, 1970)] we also investigated the following alternative emittance calibration procedure. A crystal of sodium sulfate was placed on the ribbon and the ribbon surface temperature increased by electrical heating. The brightness temperature of the ribbon at which the $Na_2SO_4(s)$ was just observed to melt was measured with an optical pyrometer. From the literature value for the $Na_2SO_4(s)$ melting point [1,157 K at 1 atm (Weast, 1975)] the 0.65 μm spectral emittance of platinum in air at high temperature was estimated to be 0.406. Using this value a new calibration curve relating Pt electrical resistance to its true surface temperature was obtained and used to construct Figure 8. Figure 8 shows theoretical prediction of the B_2O_3-deposition rates based on the assumptions that:

1) The mainstream is in complete *LTCE* at the adiabatic flame temperature. Theoretical B_2O_3 deposition rates with the mainstream at the *measured* gas temperatures (Figure 2) were found to differ from these estimates by less than 2%.

2) At the target $(HBO_2)_3$ is disallowed.

3) *BL* diffusive mass transfer is primarily Fickian, i.e., thermal diffusion is neglected. Similar theoretical calculations of mass deposition rates in combustion systems (Rosner, et al., 1979a) reveal an appreciable effect of thermal diffusion only for higher molecular weight species (e.g., $Na_2SO_4(g)$), or very *light* species (e.g., Na(g)).

If the absolute Sherwood numbers and the corresponding Fick diffusion coefficients were accurately known, Eqs. 3 to 5 could then be used to predict the B_2O_3-mass deposition rates at each surface temperature and seed level. Unfortunately, accurate Sherwood numbers for the front surface of a ribbon in crossflow at intermediate Reynolds numbers (about 60 encountered here) are not readily available and, moreover, there is considerable uncertainty about values of the diffusion coefficients for the major boron-containing species, specifically, HBO_2. (Diffusion coefficient estimates for HBO_2 at high temperature based on well-established correlations of Lennard-Jones interaction potential parameters with condensed-phase properties are clearly not possible for HBO_2, Appendix A.) Therefore, to proceed with the quantitative discussion of our B_2O_3 deposition rates, the following less

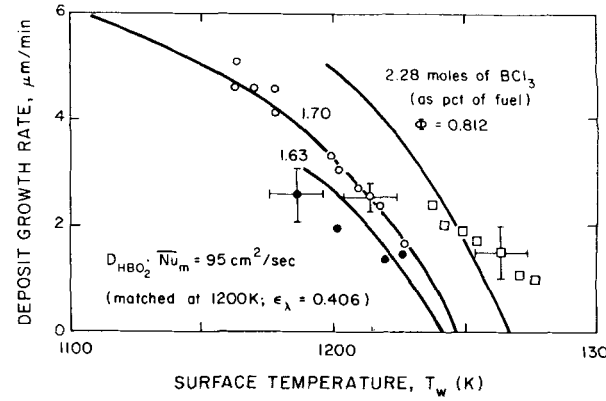

Figure 8. Experimental measurements (with target temperatures calculated using 0.406 for the spectral emittance of platinum) of $B_2O_3(l)$ film growth rates. Solid curves are theoretical predictions of $B_2O_3(l)$ deposition rates (Appendix B).

direct method was used (Appendix A). A particular value for the product of the Sherwood number and Fick diffusion coefficient was obtained by equating the righthand side of Eq. 5 to the experimentally inferred B_2O_3 mass deposition rate at one surface temperature and seed level (1,215 K and 1.7% mol BCl_3 per mol of fuel, Figure 8, respectively). Then, using this value for the $D{\cdot}Nu_m$ product, the expected deposition rates at other target temperatures and seed levels were computed. In Appendix A we show that our best present estimates for the HBO_2-dimensionless mass transfer coefficient and HBO_2-mixture diffusion coefficient are consistent with the $D{\cdot}Nu_m$ product inferred from our data. As shown in Figure 8, our theoretical predictions of the *shape* of the deposition rate vs. surface temperature relation also agree with our experimental measurements, particularly at the seed level corresponding to 1.7 mol pct. BCl_3 per mol of fuel. Significantly, at this seed level the experimental uncertainties turned out to be much less than at the other seed levels investigated here (the surface of platinum ribbons used for these particular experiments was smoother, resulting in smaller uncertainties in the measured film growth rate, although the uncertainty in the temperature inferred from electrical resistance measurement is unchanged). [Our optical interference method for measuring high-temperature deposition rates requires that the surface be sufficiently smooth, perhaps the most serious restriction on this technique. Deposition and evaporation rate measurements based on the change in polarization of the reflected light ("ellipsometry") are reported elsewhere (Seshadri and Rosner, 1984).] The resulting overall agreement supports the validity of this approach to deposition rate predictions in combustion systems containing inorganic impurities.

Other models, in which we attributed the small discrepancy between the measured and predicted *dew point* to partial equilibrium for certain species, were also investigated. In one such model we assumed that the concentration of metaboric acid vapor, $HBO_2(g)$ was less than the equilibrium value—the actual concentration being chosen to make the theoretical dew point agree with the experimental value. Corresponding $-\dot{m}'' \leftrightarrow T_w \rightarrow$ predictions (Figure 4) also reveal agreement which is quite acceptable. Again, the product of the HBO_2(g)-Fick diffusion coefficient and the prevailing Sherwood number was chosen such that the theoretical deposition rate agreed with the experimental value at one target temperature and seed level (T_w = 1,240 K and 1.7% mol BCl_3 per mol of fuel, Figure 4, respectively) and then the expected rates at other target temperatures and seed levels were obtained using this same $D{\cdot}Nu_m$ value. Because each of the above-mentioned models gives acceptable agreement (well within the uncertainty limits for our experimental measurements and theoretical predictions), it is difficult to decide which model best represents reality. However, because the first (ϵ_λ(Pt) = 0.406) model does not place any kinetic restrictions on *BL* species by bimolecular reactions, it is, perhaps, the more plausible of the two, implying that all reported ribbon temperatures (Figures 4, 5 and 6) should be corrected from ϵ_λ(Pt) ≈ 0.3 to 0.406.

Dew Point Variation with Equivalence Ratio

Figure 6 shows that at constant BCl_3 seed level, the observed variation of the measured B_2O_3 dew point with ϕ does not match the simple constrained-LTCE prediction precluding $(HBO_2)_3$ formation at the target surface. These differences may be indicative of kinetic restrictions on the homogeneous rate of formation of B_2O_3(g) at different ϕ-values. This hypothesis follows from our observation that if one writes all of the independent elementary chemical reactions capable of forming $B_2O_3(g)$ and estimates their forward rates using the equilibrium composition (calculated at the inferred gas temperature T_∞) in the law of mass action, then the ϕ dependence of the $B_2O_3(g)$-formation rate is similar in shape to the dew point data shown in Figure 6.

[Figure 9 shows that the difference in the ϕ-dependence of the calculated *adiabatic* flame temperature and the *measured* gas temperature is a consequence of gas heat loss to the burner when the gas flow rate into the burner is nearly the same for all values of ϕ. Using an overall energy balance and our thermocouple measurements, estimates of the heat loss as a function of ϕ were made via LTCE-predicted relative concentrations of major species in the flame at these temperatures, and their respective heats of formation. The ϕ-dependence of this inferred burner heat loss curve was indeed found to be nearly the same as those measured directly by Botha and Spalding (1954).]

Although such gas-phase kinetic estimates are necessarily crude, the hypothesis that dew points approximately "track" the relative rate of formation of the condensible compound when the *LTCE* mainstream is rapidly cooled to the target surface temperature suggests that homogeneous kinetic restrictions on *BL* bimolecular reactions involving the "trace" inorganics may influence the observed dew point in other situations of

Invoking *BL* nonequilibrium chemistry to explain observed dew point trends at first sight casts doubt on the self-consistency of applying

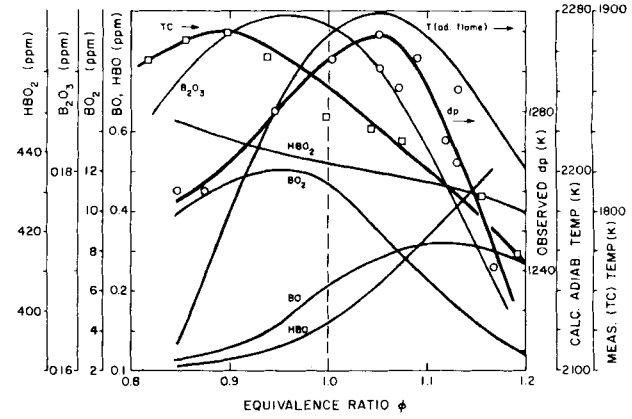

Figure 9. Theoretically calculated mainstream concentrations of the major boron-containing species in the flame at the prevailing (near-adiabatic) flame temperature as a function of ϕ. Also shown are *measured* gas temperature, and *measured* B_2O_3 dew points and calculated adiabatic flame temperatures.

CFBL-theory to interpret B_2O_3 deposition rates below the dew point. However, in vapor transport systems in which the individual trace species Lewis numbers do not depart appreciably from each other and from unity, deposition rates can be quite insensitive to *gas-phase* nonequilibrium, provided *surface* reactions establish the same overall element mass fraction *BL* driving forces. Moreover, for target temperatures well below the dew point, the tendency to "freeze" the homogeneous chemistry should intensify. This situation, coupled with a) the relative ease of making *CFBL* predictions, and b) the apparent success of CFBL theory, justifies its use here to interpret observed film growth rates from atmospheric pressure combustion gases.

CONCLUSIONS

To circumvent the need for lengthy "post-mortem" gravimetric experiments (often complicated by the onset of condensate run-off phenomena) in developing a realistic deposition rate and dew point theory, we have carried out a number of optically probed target/seeded burner experiments, and ancillary theoretical calculations, with the following principal and conclusions:

1. Laser optical reflectance techniques can be extended to combustion systems by remotely probing reflective targets for the onset of condensation "dew-point" determination). The resulting dew point is not a simple thermodynamically dictated quantity, and, in the present experiments, is evidently influenced by the kinetics of both *heterogeneous* reactions [$(HBO_2)_3$-formation] and *homogeneous* reactions [B_2O_3-formation in the quenched boundary layer gases].

2. The optical interference technique can be extended to rapidly acquire *deposition rate* information in combustion systems leading to continuous, transparent condensates [$B_2O_3(l)$ in the present case]. Using He-Ne laser beam probing and solid-state photocells for reflected light intensity measurements, this technique is simple, relatively inexpensive, and insensitive to parametric uncertainties (e.g., condensate refractive index). Moreover, such rate measurements can be achieved at liquid film thicknesses well below the onset of complicating surface flow (run-off) phenomena (Appendix B).

3. Observed trends for the dependence of the "pre-run-off" $B_2O_3(l)$-layer growth rate on both seed level and target temperature are in approximate accord with the predictions of a recently developed chemically frozen boundary layer vapor deposition (*CFBLVD*) theory. An essential feature of this theory (Rosner et al., 1979a) is the inclusion of multicomponent vapor species transport, because the condensate ($B_2O_3(l)$ in the present case) generally grows as the result of the transport of many vapor species of different stoichiometry [mainly $HBO_2(g)$ here].

4. While thermal (Soret) diffusion mass transport does not play an important role in determining dew points and deposition rates in the present experimental (B_2O_3-growth from vapor precursors)

situation, our laser-based methods and theoretical formulation lend themselves well to the systematic study and inclusion of inevitable Soret transport effects (Rosner, 1980).

In considering immediate applications and extensions of this research, it should be realized that surface quality may render the presently developed optical interference technique impractical for inferring deposition rates in some systems, even when nearly transparent thin films are involved. In this respect, the polarization method ("ellipsometry") may be more "forgiving," also admitting the possibility of measuring submicron-film *evaporation* rates (Seshadri and Rosner, 1984). We are also extending optical methods to the on-line measurement of solid aerosol initial deposition rates, using the resulting loss in specular reflection or growth of the diffuse reflection signal (Rosner and Atkins, 1983).

In summary, we hope that these optical techniques, here applied to a simple, relatively well-characterized combustion system, will provide: a) experimental data for the further development of *BL*-mass transfer predictive methods; the basis for b) an improved understanding of dew point and deposition rate phenomena in operational devices (engines, furnaces) and simulation test facilities; and c) the basis for a family of new, on-line control instruments (dew point, deposition rate transducers).

Taken together with parallel work on the development of multicomponent vapor convective transport theory (Rosner, et al., 1979a), and aerosol capture theory (Rosner et al., 1979c; Fernandez de la Mora and Rosner, 1980; Rosner et al., 1983b), it should ultimately be possible to more rationally predict and optimize the performance of practical combustion devices with respect to the phenomenon of inorganic salt/ash deposition and its corrosion consequences. Such guidance would be timely and, indeed, appears to be long overdue.

ACKNOWLEDGMENTS

It is a pleasure to acknowledge G. C. Fryburg, F. J. Kohl, C. Lowell, C. A. Stearns, P. C. Nordine, R. Atkins, and S. S. Kim for their advice and technical assistance. This work was supported by NASA-Lewis Research Center, Materials Division, under Grants NSG 3169 and NAG 3-201. A portion of the experimental equipment, also used for optical experiments of small particle deposition rates, was supported under AFOSR Contract F 49620-76-C-0020.

LITERATURE CITED

Boll, R. H., and H. C. Patel, "The Role of Chemical Thermodynamics in Analyzing Gas-Side Problems in Boilers," *ASME J. Eng. Power*, **83A**, 451 (1961).

Botha, J. P., and D. B. Spalding, "The Laminar Speed of Propane/Air Mixtures with Heat Extraction from the Flame," *Proc. Royal Soc., Ser. A*, **225**, 71 (1954).

Brown, T. D., "The Deposition of Sodium Sulfate from Combustion Gases," *J. Inst. Fuel*, **39**, 378 (1966).

DeCrescente, M. A., and M. S. Bornstein, "Formation and Reactivity Thermodynamics of Sodium Sulfate with Gas Turbine Alloys," *Corrosion*, **24**, 127 (1968).

Dicks, J. B., L. W. Crawford, C. K. Petersen, and M. S. Beaton, "Corrosion and Deposits in MHD Generator Systems," *Ash Deposits and Corrosion Due to Impurities in Combustion Gases*, R. W. Bryers, Ed., Hemisphere Publishing Corp., 651 (1977).

Fage, A., and F. D. Johansen, "On the Flow of Air Behind an Inclined Flat Plate of Infinite Span," *Proc. Royal Soc.*, Ser. A, **116**, 170 (1927).

Fernandez de la Mora, J., and D. E. Rosner, "Inertial Deposition of Particles Revisited and Extended; Eulerian Approach to a Traditionally Lagrangian Problem," *J. Physicochemical Hydrodynamics*, **2**, No. 1, 1 (1981).

Fernandez de la Mora, J., and D. E. Rosner, "Effects of Inertia on the Diffusional Deposition of Small Particles to Spheres and Cylinders at Low Reynolds Numbers," *J. Fluid Mechanics*, **125**, 379 (Dec., 1982).

Fryburg, G. C., and H. M. Petrus, "Kinetics of the Oxidation of Platinum," *J. Electrochemical Soc.*, **108**, 496 (1961).

Geiss, V., and E. Fröschle, "Mass Spectrometric Investigation of the Reaction Velocities of BCl_3 and BBr_3 with Oxygen and Water Vapor in a Diffusion Furnace," *J. Electrochemical Soc.*, **123**, No. 1, 133 (1976).

Gordon, S., and B. J. McBride, "Computer Program for Calculation of Complex Chemical Equilibrium Compositions, Rocket Performance, Incident and Reflected Shocks, and Chapman-Jouguet Detonations," NASA SP-273, Interim Rev. (1976), National Aeronautics and Space Administration, Washington, DC (1971).

Halstead, W. D., and E. Raask, "The Behavior of Sulfur and Chlorine Compounds in Pulverized Coal Fired Boilers," *J. Inst. Fuel*, **42**, 344 (1969).

Heywood, J. B., and G. J. Womack, *Open-Cycle MHD Power Generation*, Pergamon Press, Oxford, U.K. (1969).

Hedley, A. B., T. D. Brown, and A. Shuttleworth, "Vanadium Pentoxide Deposition from Combustion Gases," *Trans. ASME, J. Eng. for Power, Ser. A*, **88**, 173 (1966).

Hirschfelder, J. O., C. F. Curtiss, and R. B. Bird, *The Molecular Theory of Gases and Liquids*, John Wiley and Sons, New York (1954).

Israel, R., "Thermal Diffusion Effects on Fuel Vapor Mass Transport Across Non-Isothermal Boundary Layers in Surface Catalyzed Combustion," Ph.D. Dissertation, Yale University, (Spring, 1983).

Jackson, P. J., "Deposition of Inorganic Material in Oil-Fired Boilers," *Ash Deposits and Corrosion Due to Impurities in Combustion Gases*, R. W. Bryers, Ed., Hemisphere Publishing Corp., 147 (1977).

Kays, W. M., and M. E. Crawford, *Convective Heat and Mass Transfer*, McGraw-Hill, New York (1980).

Kent, J. H., "A Noncatalytic Coating for Platinum-Rhodium Thermocouples," *Combustion and Flame*, **14**, 279 (1970).

Kohl, F. J., G. J. Santoro, C. A. Stearns, G. C. Fryburg, and D. E. Rosner, "Theoretical and Experimental Studies of the Deposition of Na_2SO_4 from Seeded Combustion Gases," *J. Electrochemical Soc.*, **126**, 1054 (1979).

Laxton, J. W., C. G. Stevens, and D. Tidy, "Deposition of Sodium Compounds Under Gas Turbine Conditions," Central Electricity Generating Board—CERL (Leatherhead, Surrey, U.K.), Final Report (NTIS NC A03/MF A01) (1978); *J. Inst. Energy*, **3**, 3 (March, 1981).

Lyman, T., Ed., *Metals Handbook: Properties and Selection of Metals*, 8th Ed., 1, American Soc. for Metals, Metals Park, OH (1975).

McAdams, W. H., *Heat Transmission*, 3rd Ed., McGraw-Hill Co., New York (1954).

McIntyre, R. J., and F. K. McTaggart, "Comparison of the Reactions of Atomic and Molecular Halogens with Silver," *J. Phys. Chem.*, **74**, 866

Meschi, D. J., W. A. Chupka, and J. Berkowitz, "Heterogeneous Reactions Studied by Mass Spectrometry. 1. Reaction of $B_2O_3(s)$ with $H_2O(g)$," *J. Chem. Phys.*, **33**, No. 2, 530 (1960).

Nordine, P. C., D. E. Rosner, and P. J. Kindlmann, "New Methods for Studying Gas—Solid Reaction Kinetics Using Automated Resistance Monitoring," *Rev. Sci. Instrum.*, **44**, No. 7, 821 (July, 1973).

Prausnitz, J. M., C. A. Eckert, R. V. Orye, and J. P. O'Connell, *Computer Calculations for Multicomponent Vapor-Liquid Equilibria*, Prentice-Hall, Englewood Cliffs, NJ (1967).

Rosner, D. E., "Multicomponent Mass Transfer from Combustion Gases," 73rd Annual Meeting of AIChE, Chicago (Nov. 1980b).

Rosner, D. E., "Thermal (Soret) Diffusion Effects on Interfacial Mass Transport Rates," *J. Physicochemical Hydrodynamics*, Pergamon Press, **1**, No. 2, 159 (1980).

Rosner, D. E., and R. M. Atkins, "Experimental Studies of Salt/Ash Deposition Rates from Combustion Products Using Optical Techniques," *Proc. Engineering Foundation Int. Conf. on Experimental Research into Fouling and Slagging Due to Impurities in Combustion Gases* (1983) pp 469–492.

Rosner, D. E., B. K. Chen, G. C. Fryburg, and F. J. Kohl, "Chemically Frozen Multicomponent Boundary Layer Theory of Salt and/or Ash Deposition Rates from Combustion Gases," *Combus. Sci. and Tech.*, **20**, 87 (1979a).

Rosner, D. E., and M. Epstein, "Fog Formation Conditions Near Cool Surfaces," *J. Colloid and Interface Sci.*, **28**, 60 (1968).

Rosner, D. E., and J. Fernandez de la Mora, "Small Particle Transport Across Turbulent Non-Isothermal Boundary Layers," *ASME Trans., J. Engineering for Power*, **104**, No. 4, 885 (1982).

Rosner, D. E., S. Gokoglu, and R. Israel, "Rational Engineering Correlations of Diffusional and Inertial Particle Deposition Behavior in Non-Isothermal Forced Convection Environments," *Proc. Engrg. Foundation Int. Conf. on Fouling of Heat Exchange Surfaces* (1983).

Rosner, D. E., D. Günes and N. Anous, "Aerodynamically-Driven Condensate Layer Thickness Distributions on Isothermal Cylindrical Surfaces," *Chem. Eng. Commun. 24*, 275–287 (1983).

Rosner, D. E., and R. Nagarajan, "Transport-Induced Shifts in Condensate Dew Point and Identity in High Temperature Multicomponent Systems with Chemical Reaction," Chemical Engineering Science (in press, 1984).

Rosner, D. E., and K. Seshadri, "Experimental and Theoretical Studies of the Laws Governing Condensate Deposition from Combustion Gases," *18th Symp. (International) on Combustion*, Comb. Inst., Pittsburgh, Pa (1981), pp. 1385–1394.
Rosner, D. E. et al., "Transport, Thermodynamic and Kinetic Aspects of Salt/Ash Deposition Rates from Combustion Gases," *Proc. 10th Materials Research Symposium: Characterization of High Temperature Vapors and Gases*, NBS Special Pub. #561, 1451 (1979b).
Samsonov, G. V., *The Oxide Handbook*, Plenum Press, New York (1973).
Schlicting, H., *Boundary Layer Theory*, McGraw-Hill, New York (1960).
Seshadri, K., and D. E. Rosner, "Polarization (Ellipsometric) Measurement of Condensate Deposition and Evaporation Rates, and Dew Points in Salt/Ash-Containing Combustion Gases," *Combustion and Flame* (in press (1984)).
Smithells, C. J., *Metals Reference Book*, III, 4th Ed., Plenum Press, New York (1967).
Stearns, C. A., F. J. Kohl, and D. E. Rosner, "Combustion System Processes Leading to Corrosive Deposits," DOE/NASA/2593-27, NASA TM-81752, *Proc. Int. Conf. On High Temp. Corrosion* (1983).
Stringer, J., "Hot Corrosion of High Temperature Alloys," *Ann. Rev. of Mat. Sci.*, **7**, R. A. Huggins, Ed., Annual Reviews, Inc., Palo Alto, CA, 477 (1977).
Stull, D. R., and H. Prophet, Project Ed., *JANAF Thermochemical Tables*, 2nd Ed., National Bureau of Standards, U. S. Department of Commerce, Washington, DC (1971)
Sugawara, K., T. Yoshimi, H. Okuyama, and T. Shirasu, "Monitoring of CVD Film Thickness by Laser System," Fourth Int. Conf., Electrochemical Soc., Princeton, NJ. 205 (1973).
Touloukian, Y. S., and D. P. DeWitt, *Thermophysical Properties of Matter*, **7**; *Thermal Radiative Properties, Metallic Elements and Alloys*, Plenum Press, New York (1970).
Touloukian, Y. S., and D. P. DeWitt, *Thermophysical Properties of Matter*, **8**; *Thermal Radiative Properties Nonmetallic Solids*, Plenum Press, New York (1972).
Washburn, E. W., Ed., *International Critical Tables of Numerical Data for Chemistry and Technology*, **6**, McGraw-Hill (1933).
Weast, R. C., Ed., *Handbook of Chemistry and Physics*, 55th Ed., CRC Press, Cleveland, OH (1975).

Manuscript received September 10, 1979; revision received March 15, 1983 and accepted April 1, 1983.

APPENDIX A: PREDICTION OF MASS DIFFUSIVITIES AND TRANSFER COEFFICIENTS

Predictions of the $B_2O_3(l)$ deposition rate (Figures 4 and 8) are based on the *CFBL* theory of Rosner et al. (1979a). Although, in principle, all boron-containing vapor species contribute to the deposition of boric oxide, in our present experiments the dominant term is found to be that of $HBO_2(g)$, with the remaining small fractions being primarily due to $BO_2(g)$, and $B_2O_3(g)$. Therefore, to fix ideas, we here consider prediction of the Sherwood number, $Nu_{m,i}$, to the front face of a ribbon in cross-flow, and the pseudobinary coefficient of diffusion $D_{i\text{-mix}}$, for $i = HBO_2(g)$. We will then examine whether the film growth measurements reported earlier are consistent with expected values of the $D_{HBO_2\text{-mix}} \cdot Nu_{m,HBO_2}$ product.

Since, to our knowledge, no direct experimental measurements of Nu_m for the front face of a ribbon in cross-flow exist at the values of the Reynolds and Schmidt numbers used in our experiments (about 57 and 0.78, respectively) an indirect procedure must be used. One possible route is to evaluate $Nu_{m,i}$ at high Reynolds number $[(Re)^{1/2} \gg 1]$ and then extrapolate the result to "low" Reynolds number. For this purpose, early measurements of the *pressure* distribution on the front face of a transverse flat plate in cross-flow at high Reynolds number (about 2×10^5) (Fage and Johansen, 1927) were used to calculate the corresponding inviscid velocity distribution (via Bernoulli's theorem) and, in particular, the velocity gradient (du_e/dx) at the forward stagnation line $x = 0$ was found to be $1.327\ U/l$ (where l is the total ribbon width). From well-known results for the stagnation-line value $Nu_m(0)$ from laminar boundary layer (*LBL*) theory (Kays and Crawford, 1980), we therefore estimate:

$$Nu_{m,i}(0) = 0.6565\ Re^{1/2}(Sc_i)^{0.4} \quad (Re^{1/2} \gg 1) \quad \text{(A1)}$$

where the coefficient $(0.6565 = 0.570(1.327)^{1/2})$ is about 15% *lower* than that expected if we averaged over the entire front surface. However, in the absence of appreciable shear-driven condensate flow (Appendix B) the latter (front-surface average Nu_m) is *not* required. Unfortunately, there is no simple procedure to extrapolate the high Reynolds number asymptotic result given by Eq. A1 to the "low" Reynolds numbers characteristic of our experiments. Existing data for the surface-averaged coefficient of *heat* transfer for flow over a circular cylinder in cross-flow (McAdams, 1954) indicate that the coefficient appearing in the expression for this quantity, as well as the *Re*-exponent, increase with Reynolds number. But, if the Nu_m ratio at low and high Reynolds numbers were about the same for the ribbon as for the circular cylinder we would estimate that in the present case:

$$Nu_{m,i}(0) \approx 4.3(Re)^{1/2}\cdot(Sc_i)^{0.4} \quad (Re \approx 60) \quad \text{(A2)}$$

These "constant property" nondimensional mass transfer coefficients should be corrected for the modest systematic effects of temperature-induced variable gas mixture properties (Srivastava and Rosner, 1979). This amounts to the multiplication of Eqs. A1 and A2 by a factor of the order of $C_{mh}\cdot(T_w/T_e)^{0.1}$, estimated to be about 0.88 in the present case. Without access to Oseen-flow calculations for ribbons in cross-flow, or direct front surface *Nu*-data at intermediate Reynolds' numbers, we conclude that for the present experimental conditions only rough *a priori* Nu_m estimates can be made on the basis of high Reynolds number *LBL* theory.

The situation regarding *a priori* predictions of diffusion coefficients is somewhat more favorable. The pseudobinary diffusion coefficient of HBO_2 in the prevailing combustion gas mixture can be computed from

$$D_{HBO_2\text{-mix}} = (1 - y_{HBO_2})\cdot\left(\sum_j y_j/D_{HBO_2\text{-}j}\right)^{-1} \quad \text{(A.3)}$$

where subscript j pertains to the major components of the product gas mixture, y is the mole fraction, and $D_{HBO_2\text{-}j}$ is the binary diffusion coefficient of HBO_2 with species j. Well-known correlations for estimating the binary diffusion coefficients using the Chapman-Enskog theory (Hirschfelder et al., 1954) are not usable because stable condensed phases do not exist for the species HBO_2 on which one could base Lennard-Jones 12:6 potential parameter estimates. For some compounds a practical alternative is to estimate these based on known values for "similar" compounds. For example, BO_2-parameters can be based on their counterparts for, say CO_2 and NO_2 (Svehla, 1962). On this basis, $D_{BO_2\text{-}j}$ and $D_{BO_2\text{-mix}}$ were estimated. The case of $D_{HBO_2\text{-mix}}$ is less clear and, in the absence of more direct information, we simply assumed $D_{HBO_2\text{-mix}} \approx D_{BO_2\text{-mix}}$ ($\approx 4.5 \times 10^{-4} m^2/s$ at 1,900 K and 1 atm).

The remaining quantities needed are more certain. Here we assumed the density of the gas mixture at $\phi = 0.8175$, $T_e = 2{,}040$ K, 1 atm to be 1.78×10^{-1} kg·m^{-3} and 0.626×10^{-4} Pa·s, respectively. The value of 1.8×10^3kg·m^{-3} for the density of $B_2O_4(l)$ was obtained from the compendium of Samsonov (1973). Based on ribbon width (6 mm) the Reynolds number was estimated as 57 and the HBO_2 Schmidt number about 0.78. Using all of the above-mentioned estimates we expect the product $10^4\ (D_{HBO_2}\cdot Nu_{m,HBO_2})_e$ to be between 26 and about 117 m^2·s^{-1}, being closer to the latter at $Re \approx 57$. Fitting our experimental data at one point and assuming $\epsilon_\lambda(Pt) = 0.4$ yields 76 m^2·s^{-1}, whereas our alternate model based on incomplete $HBO_2(g)$ formation yields 96 m^2·s^{-1}. Thus, both the experimentally observed film-growth *trends* (with target temperature and seed level) and the *absolute values* of the observed film-growth rates are evidently consistent with out basic *BLVD*-approach and the absence of condensate flow phenomena on the target (Appendix B).

APPENDIX B: ASSESSMENT OF CONDENSATE FLOW EFFECTS

The *film* growth rate yields the deposition mass flux directly only if we can neglect the condensate film flow ("run-off") that will

inevitably result from aerodynamic shear (x-direction) and/or surface tension gradients (ribbon spanwise (z) direction). We show below that the present optical interference results on $B_2O_3(l)$ film growth rates are obtained at film thicknesses (about 1 μm) well below the onset of flow due to either aerodynamic shear or surface tension gradients. Perhaps the simplest way of demonstrating this is to compare the film growth rate produced by local deposition (from the vapor phase) to the growth rates that would be produced by each rival mechanism if acting alone.

Aerodynamic Shear-Induced Condensate Flow

If *the deposition process* were instantaneously "turned off," the prevailing aerodynamic shear-induced condensate flow would cause the stagnation point liquid film thickness to *decrease* at the instantaneous rate:

$$\left(-\frac{\partial \delta_l}{\partial t}\right)_{\text{gas shear}} \cong \frac{1}{2\mu_l} \cdot \left(\frac{\partial \tau_{yx}}{\partial x}\right)_{\substack{x=0 \\ y=0}} \cdot \delta_l^2 \qquad \text{(B1)}$$

This special case is readily derived from the more general mass and momentum conservation equations governing laminar Newtonian-fluid thin-film dynamics, quantitatively treated in Rosner, Günes and Anous (1983).

Using laminar *BL* theory (Howarth-Blasius series method, Schlicting, 1960) to estimate $(\partial \tau_{yx}/\partial x)_{x=0,y=0}$ via the above-mentioned value of $(du_e/dx)_{x=0}$ (Appendix A), and estimating the $B_2O_3(l)$ viscosity, $\mu_l \{T_w\}$ (about 10 Pa·s) from the compendium of Samsonov, 1973, we find what when $\delta_l \approx 1$ μm the absolute value of this contribution is smaller than the observed $\partial \delta_l/\delta t$ by over four decades. Thus, only at $B_2O_3(l)$ film thicknesses well above 10 μm would this mechanism begin to play a role in the interpretation of $B_2O_3(l)$ film growth rate measurements.

Surface-Tension Gradient-Induced Condensate Flow

Condensate flow induced via spanwise temperature gradients in the ribbon can be treated in an analogous manner, where $(d\sigma/dT)\cdot(\partial T_w/\partial z)$ plays the role of the aerodynamic shear stress $(\tau_{yx})_w$. Accordingly, we estimate:

$$\left(\frac{\partial \delta_l}{\partial t}\right)_{\text{grad } \sigma} \cong \frac{1}{2\mu_l} \cdot \left(-\frac{d\sigma}{dT}\right)\left(\frac{\partial^2 T_w}{\partial z^2}\right)_{z=0} \cdot \delta_l^2 \qquad \text{(B2)}$$

Our spanwise ribbon temperature measurements indicate that under experimental deposition conditions $\partial^2 T_w/\partial z^2$ is of the order of -260 K/cm^2 and, in our target temperature range available measurements on $B_2O_3(l)$ (Kingery, 1959) indicate $d\sigma/dT \approx +0.55 \times 10^{-4}$N·m^{-1}·K^{-1} (note the sign!). Therefore, the magnitude of this contribution at $\delta_l \approx 1$ μm is smaller than our observed $\partial \delta_l/\partial t$ values by about four decades.

On the basis of these estimates (Eqs. B1 and B2), we conclude that our interferometrically deduced $B_2O_3(l)$ film growth rates yield local deposition mass fluxes without the need for corrections associated with condensate surface flow effects. As a corollary, effects due to condensate flow *cannot* be the cause of any systematic differences between the $D_{HBO_2}Nu_{m,HBO_2}$ product estimated *ab initio* (from available literature data) and that inferred by fitting our own $\partial \delta_l/\partial t$ data at one point, using *CFBL* vapor deposition theory (Appendix A). Rather, the modest differences found (i.e., usually agreement to within better than a factor of about 1.5) are readily accounted for by present uncertainties in: a) the low Reynolds number effect on the prevailing dimensionless mass transfer coefficient (for a ribbon in cross-flow); and b) the collisional parameters governing the diffusion coefficient of vapor species like $HBO_2(g)$.

NOTATION

C_{mh} = correlating factor for effect of variable properties on mass and heat transfer coefficients
d = diameter of thermocouple bead
D_i = Fick (or Brownian) coefficient for diffusion of species i
j_i'' = diffusional mass flux of species i
l = total width of ribbon target ($\perp$ span)
L = characteristic (reference) dimension of target
$-\dot{m}_{i,w}''$ = deposition mass flux of chemical species i
Nu_m = Sherwood number (Nusselt number for *mass* transport)
n = refractive index of condensate film [$B_2O_3(l)$ in present experiments]
Re = characteristic Reynolds number for the viscous gas flow
Sc_i = Schmidt number, ν/D_i
T = absolute temperature
T_∞ = mainstream gas temperature
U = velocity of the gas stream
x = streamwise distance along target surface ($\perp$ span)
y_i = mole fraction of chemical species i
z = distance along target span (Appendix B)

Greek Letters

α_i = nondimensional thermal diffusion factor, Eq. 2
δ_l = liquid condensate layer thickness at measurement location
$\Delta\delta_l$ = increment in condensate film thickness, Eq. 1
ϵ_λ = target emittance at wavelength λ
θ = angle of incidence (laser probe beam)
λ = wavelength of laser light (0.6328 μm)
ν = kinematic viscosity (momentum diffusivity), μ/ρ
ρ = density (gas mixture, unless otherwise specified)
ϕ = equivalence ratio(=(fuel/air)ratio/stoichiometric (fuel/air)ratio)
ω_i = mass fraction of species i
μ_l = dynamic viscosity of liquid condensate
σ = surface tension of liquid condensate
τ_{yx} = yx component of viscous stress tensor
$\omega_{B/i}$ = fraction of the mass of molecule i contributed by the element boron

Subscripts

(B) = element boron
dp = dew point
e = outer edge of boundary layer
i = species i
w = target surface or gas/condensate interface
l = pertaining to liquid film
mix = pertaining to prevailing gas mixture
∞ = in gas "far" upstream of collector

Miscellaneous

grad = spatial gradient operator, Eq. 2
(l) = liquid phase
(g) = gas phase

Abbreviations

BL = boundary layer
CF = chemically frozen (source-free)
GT = gas (combustion) turbine
LTCE = local thermochemical equilibrium
TC = thermocouple
VD = vapor deposition
VLE = vapor/liquid equilibrium